magnetism

MDPI

Article

Competing Magnetic Interactions in Inverted Zn-Ferrite Thin Films

Murtaza Bohra [1,*], Sai Vittal Battula [1], Nitesh Singh [1], Baidyanath Sahu [1], Anil Annadi [1] and Vidyadhar Singh [2]

[1] École Centrale School of Engineering (MEC), Mahindra University, Hyderabad 500043, India; saivittal18238@mechyd.ac.in (S.V.B.); nitesh20pphy012@mahindrauniversity.edu.in (N.S.); baidyanathsahu@gmail.com (B.S.); anilannadi@gmail.com (A.A.)

[2] Department of Physics, Jai Prakash University, Chapra 841301, India; vsraj47@gmail.com

* Correspondence: murtaza.bohra@mahindrauniversity.edu.in

Abstract: Zn-ferrite is a versatile material among spinels owing to its physicochemical properties, as demonstrated in rich phase diagrams, with several conductive or magnetic behaviors dictated by its cation inversion. The strength and the type of cation inversion can be manipulated through the various thermal treatment conditions. In this study, inverted Zn-ferrite thin films prepared from radio frequency magnetron sputtering were subjected to different in situ (in vacuum) and ex situ (in air) annealing treatments. The temperature and field dependence of magnetization behaviors reveal multiple magnetic interactions compared to its bulk antiferromagnet behavior. Using the magnetic component model, the different magnetic interactions can be explained in terms of superparamagnetic (SPM), paramagnetic (PM), and ferrimagnetic (FM) contributions. At low temperatures, the SPM and FM contributions can be approximated to the hard and soft ferrimagnetic phases of Zn-ferrite, respectively, which changes with the annealing temperature and sputter power. Distinct magnetic properties emanating from in situ annealing compared to the ex situ annealing were ascribed to the nonzero Fe^{2+}/Fe^{3+} ratio, leading to the different magnetic interactions. The anisotropy was found to be the key parameter that governs the behavior of annealed in situ samples.

Keywords: magnetic interactions; cation inversion; nanocrystalline Zn-ferrite; annealing

Citation: Bohra, M.; Battula, S.V.; Singh, N.; Sahu, B.; Annadi, A.; Singh, V. Competing Magnetic Interactions in Inverted Zn-Ferrite Thin Films. *Magnetism* **2022**, *2*, 168–178. https://doi.org/10.3390/magnetism2020012

Academic Editor: Federico Spizzo

Received: 31 March 2022
Accepted: 11 May 2022
Published: 17 May 2022

1. Introduction

Zn-ferrite ($ZnFe_2O_4$) is a spinel ferrite with a chemical composition that guarantees abundant and relatively cheap production costs, in addition to its environmentally friendly nature [1–6]. Its spinel structure is relatively "open", with many vacant crystallographic sites, which facilitates the insertion of (mobile) dopants that can expand the number of applications of such material [1,2]. Zn-ferrite is very sensitive to growth conditions that can produce different amounts of defects and grain boundary densities, off-stoichiometry effects in the Zn and Fe content, nonzero Fe^{2+}/Fe^{3+} ratios, and micro/nano strains, which eventually affect the overall properties of nanostructured Zn-ferrite [7–12]. Even though thermal annealing is a convenient way for fine-tuning magnetic properties by controlling their crystallite sizes, modifying their surfaces, and affecting their magnetic interactions, it can also have detrimental effects. For instance, upon annealing, the migration of Zn cations can lead to the formation of two different crystalline (hematite and magnetite) phases along with Zn-ferrite, which eventually hinders many technological applications [6,9,13,14]. The thermodynamics of the cation disorder and the dependence of the degree of inversion with the annealing temperature have been studied in various nanostructured Zn-ferrite, ranging from nanoparticles to nanocrystalline thin films [7,15,16]. The cation inversion can be presented as $[Zn_{1-x}{}^{+2}Fe_x{}^{+3}]_A[Zn_x{}^{+2}Fe_{2-x}{}^{+3}]_BO_4$ in the inverted Zn-ferrite's tetrahedral (A) and octahedral (B) sites, in contrast to the bulk $[Zn]_A[Fe_2]_BO_4$ normal structure. Despite the fact that we know that the distribution of cations (Fe^{3+} and Zn^{2+}) governs the physical

properties of Zn-ferrite films and their emerging applications in spintronic [17] and high-frequency devices [18–23], its low-temperature magnetic properties have not been explored extensively; it is very important to understand the ordering behavior of magnetism in Zn-ferrite. In this study, inverted Zn-ferrite thin films were synthesized by sputtering, followed by in situ vacuum annealing and ex situ air annealing. These films exhibit interesting and different temperature-dependent magnetic properties, which can be explained in terms of the magnetic (ferrimagnetic, superparamagnetic, and paramagnetic) components model.

2. Experimental

Zn-ferrite thin films (500 nm) were prepared by radio frequency (RF) magnetron sputtering on fused quartz substrates at an RF power of 100 and 200 W in a pure argon pressure of 1×10^{-3} mbar from the ceramic $ZnFe_2O_4$ target. The first set of as-grown films were annealed ex situ at temperatures of 500 and 850 °C in the air for one hour. We selected these two annealing temperatures (500 and 850 °C), wherein at the former temperature, large magnetizations were reported in the literature, and for the latter temperature, a bulk normal structure was obtained [7,20]. The second sets of as-grown films were annealed in situ in the vacuum of 1×10^{-5} mbar at the annealing temperature of 500 °C for two hours. The crystalline phase and microstructure of these films were studied by X-ray diffraction (XRD) and scanning electron microscope (SEM), respectively. The magnetic properties were measured by a physical property measurement system (PPMS) attached to a vibrating sample magnetometer (VSM). The temperature dependence of magnetization (M-T) data was measured in a relatively large applied field of 1.59×10^6 A/m with cooled conditions from 300 to 5 K. The diamagnetic contribution of quartz substrate was subtracted from the magnetization data of films.

3. Results and Discussion

XRD patterns of as-grown Zn-ferrite thin films and those annealed in the air (ex situ) and vacuum (in situ) are shown in Figure 2, confirming the formation of a single-phase FCC cubic spinel Zn-ferrite structure. Significantly, XRD peaks can be observed even in as-grown samples prepared at a sputter power of 100 and 200 W, which is otherwise hardly observed in ferrite films without going through high-temperature processing [7,24]. The XRD pattern obtained for films annealed at 850 °C in the air is mostly similar to the bulk polycrystalline Zn-ferrite (JCPDS file no. 22–1012) powder. The lattice constant for these films was extracted and provided in Table 1, in the range of 8.41–8.46 Å, compared to the bulk Zn-ferrite value of 8.44 Å [25]. The larger lattice constant (8.46 Å) in the as-grown film is ascribed to the room temperature growth-induced stresses, which, however, reduces to 8.44 Å for the air-annealed (850 °C) sample. On the other hand, the Zn-ferrite films annealed in the vacuum exhibit a lower lattice constant (8.41 Å) compared to the bulk value (8.44 Å), indicating stoichiometric or Fe valence state changes [25] due to vacuum annealing, which we will discuss further in a later section. The grain sizes estimated from the Scherrer formula (Table 1) for as-grown films are in the range of 24–30 nm and increase (31–58 nm) upon annealing (irrespective of the environment), which is further supported by SEM images (see Figure 1).

Table 1. Lattice constants, grain sizes, and M-T data fitting parameters.

Sample	Lattice Constant (Å)	Grain Size (nm)	β	T_C *or* θ *(K)*	α
as-grown 100 W	8.46	24	1.25	604	0.85
as-grown 200 W films	8.43	30	1.25	600	0.8
100 W films air annealed at 500 °C	8.43	31	1.45	452	1
100 W films air annealed at 850 °C	8.44	58	-	254	0
100 W films vacuum annealed at 500 °C	8.41	41	2.5	828	1

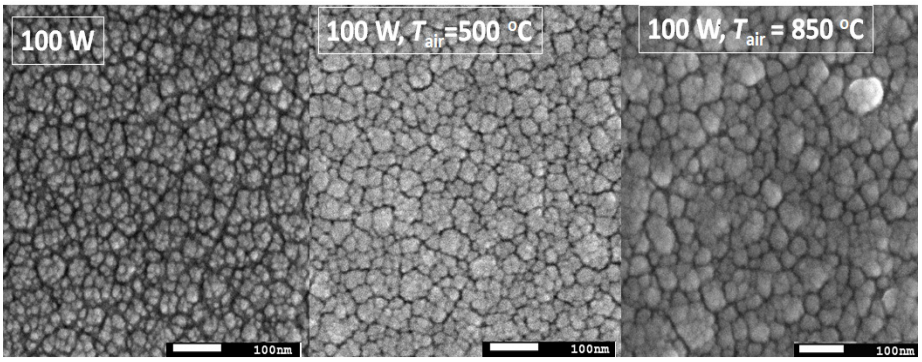

Figure 1. SEM images of as-grown Zn-ferrite thin films (deposited at an RF power of 100 W), which were later annealed at 500 °C and 850 °C in the air.

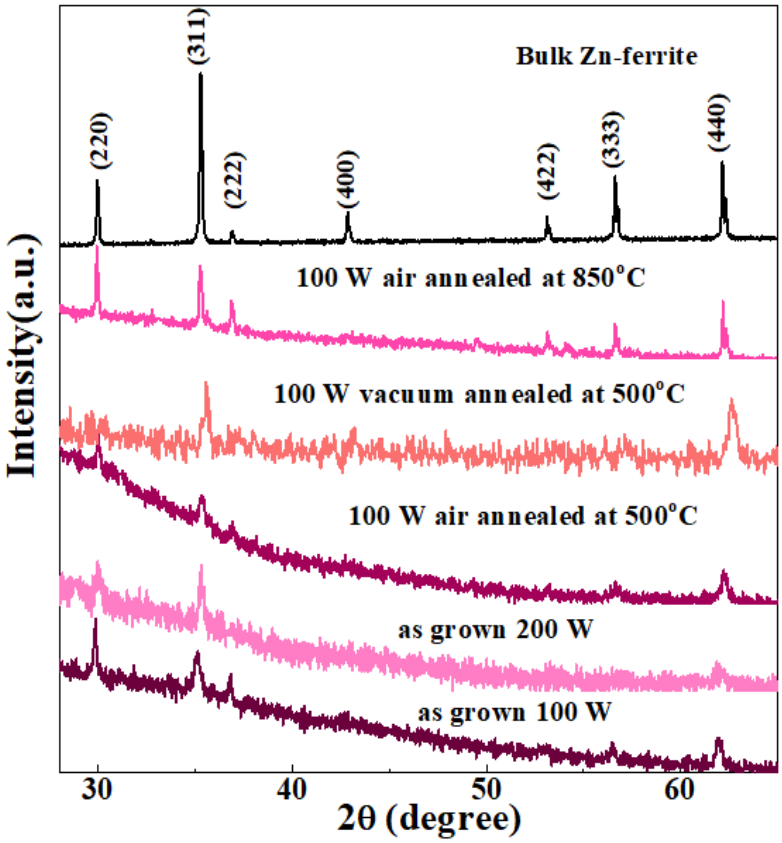

Figure 2. XRD patterns of as-grown, air-annealed, and vacuum-annealed Zn-ferrite thin films along with bulk Zn-ferrite data.

The effect of ex situ air annealing on the temperature dependence of magnetization of Zn-ferrite thin films was investigated first. The field-cooled (FC) magnetizations of as-grown and air-annealed samples are plotted in Figure 3. The magnetization behavior of the ex situ air-annealed sample shows distinct magnetization behaviors in comparison to the bulk Zn-ferrite, which is paramagnetic at room temperature and antiferromagnetic below T_N of 15 K [22]. In comparison, as-grown 100 and 200 W samples show a gradual increase of magnetization with an upturn below 50 K, indicating the mixture of superparamagnetic (SPM) and ferrimagnetic (FM) grains. While the ex situ air-annealed sample at 500 °C (sputter power of 100 W) shows the resemblance of dominant FM ferrimagnetic behavior, the ex situ air-annealed sample at 850 °C shows more paramagnetic (PM) behavior. To confirm and estimate the contribution of various magnetic interactions, FC magnetization curves were fitted to Expression (1) that consists of ferrimagnetic (FM) (first term)

and superparamagnetic (SPM) (second term) or paramagnetic (PM) functions [26–28], as given by,

$$M(T) = \alpha \left[M_S \left\{ 1 - \left(\frac{T}{T_C} \right)^{\beta} \right\} \right] + (1 - \alpha) \frac{C}{T} \quad (1)$$

where T_C is the Curie temperature, β is the critical exponent, and C is the Curie constant. The terms α and $(1 - \alpha)$ refer to the FM and SPM or PM contributions, respectively.

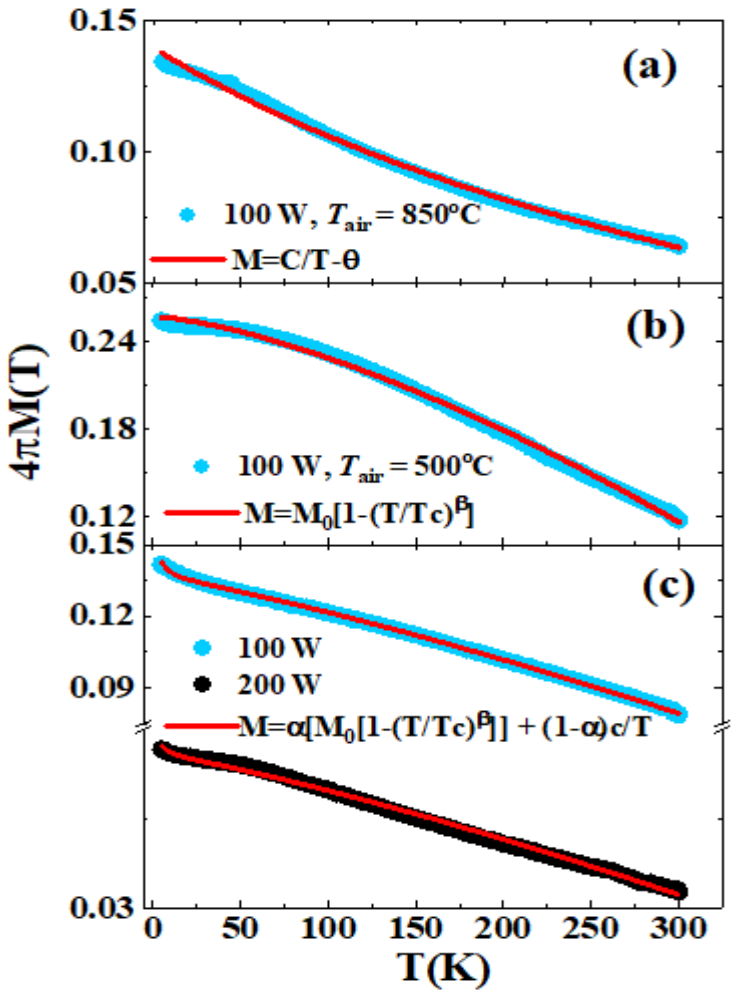

Figure 3. FC M-T curves measured at the fixed field of 1.59 × 10^6 A/m for as-grown (**a**) and air-annealed Zn-ferrite thin films (**b**,**c**). Red lines indicate fitted data with a component model.

All the extracted fitting parameters are given in Table 1. The FM contribution can be attributed to the partial inversion or mixed inverted spinel Zn-ferrite structures. The presence of smaller-sized superparamagnetic (SPM) grains, which have very low blocking temperatures, show Curie-law-type ($\sim\frac{C}{T}$) decay of the magnetization. It is estimated that the as-grown films (100 and 200 W) show 15–20% SPM contributions. The FM part can be fitted well to the ferromagnetic Bloch's law [26,27] with a β value of ~1.25 instead of a reported FM value of 1.5 and high T_C values of ~ 600 K. On the other hand, the FC curves of the sample annealed at 500 °C can be well fitted mainly with the FM part, giving β and T_C values of ~1.45 and ~452 K, respectively. This is because now smaller SPM grains also grow in size and become FM upon annealing. For a higher annealing temperature of 850 °C, the FC curve changes its shape and can now be fitted well with the Curie–Weiss (C–W) law, ~$\frac{C}{T-\theta}$, where θ is the Weiss temperature. The Weiss temperature is related to the strength and type of magnetic interactions present [28]. The yielded Weiss temperature is θ = −254 K. This large negative value reflects the presence of dominant

antiferromagnetic ordering, possibly due to the Zn-ferrite structure tending to resume its normal bulk structure. The large $\frac{\theta}{T_N} > 3$ value in our antiferromagnetic Zn-ferrite thin films suggests the existence of geometrical frustration in the compounds [28]. Recently, Monsalve et al. [21] grew sputtered Zn-ferrite thin films on Si substrates under a pure Ar gas atmosphere with an Ar/O_2 ratio of 1:2 and 2:1, showing a signature of room temperature magnetic ordering. However, they measured low-temperature magnetic properties only for the sample of Ar/O_2 (2:1), which had an extrapolated Curie temperature value of ~440 K. Our previous study [22] on nanocrystalline Zn-ferrite thin films synthesized by pulsed laser deposition (PLD) in an oxygen atmosphere (0.16 mbar) found the films were ferrimagnetic only at an intermediate in situ growth temperature (200–500 °C) while our sputtered samples were strongly ferrimagnetically ordered even at the as-grown state. On the other hand, Yamamoto et al. [23] reported that $ZnFe_2O_4$ thin films deposited at a low oxygen atmosphere (1×10^{-6} mbar) showed cluster glass behavior. Therefore, to understand these diverse results, it is imperative to conduct an in-depth investigation of magnetic properties of annealed Zn-ferrite thin films and how various SPM, FM, and PM, and/or AFM components further play a key role in determining magnetic properties at the nanoscale.

To evaluate the above distinct magnetic behaviors observed in our Zn-ferrite thin films, the field dependence of the magnetization (M−) curve was measured at a low temperature, which is shown in Figure 4 for both as-grown and air-annealed samples. The M–H curve of Zn-ferrite thin films indicated a ferrimagnetic nature, in contrast to the AFM behavior of typical bulk Zn-ferrite. The low-field region (insets) shows the nonzero remnant magnetization and coercivity values while high fields regions show a nonsaturation behavior of M–H curves even for the highest magnetic field of 6.37×10^6 A/m. This nonsaturation behavior is further pronounced in high-temperature annealed samples, indicating the increased PM/AFM contribution alike observed in FC M-T data. To quantify SPM/PM/AFM contributions along with the FM contribution, we fitted M–H curves (solid lines) with Expression (2), assuming the individual contributions of the FM, AFM, and/or PM components;

$$M(H) = \sum_{i=1}^{2} \alpha^i \left[\frac{2M_S^i}{\pi} \tan^{-1} \left\{ \frac{H \pm H_C^i}{H_C^i} \tan\left(\frac{\pi S^i}{2} \right) \right\} \right] + \left(1 - \alpha^1 - \alpha^2\right) \chi H \qquad (2)$$

here, both the first (i = 1) and second (i = 2) term is an appropriate function for fitting FM hysteresis curves [29,30], and the third term is a linear component representing a PM and/or AFM contribution. As the FC M-T curves (Figure 3) indicated as-grown films have an SPM contribution, such an SPM phase is anticipated to show FM behaviors at very low temperatures (below the blocking temperature). For this reason, second FM terms were added in Expression (2), in addition to inverted spinel FM grain contributions. Here, $S = M_r/M_S$ is the squareness ratio, Ms is the saturation magnetization, χ is the magnetic susceptibility, and H_C is the coercivity. The α^1, α^2, and $1 - \alpha^1 - \alpha^2$ are the contribution of the FM part-1 and FM part-2 and the PM or AFM part, respectively. All the extracted fitting parameters are given in Table 2. The total FM contributions are predominant in as-grown films grown at 100 and 200 W while the PM or AFM contribution increases from ~11 to ~17% with an increasing annealing temperature. This is expected because high-temperature annealing facilitates cation distribution partially reverts to the bulk Zn-ferrite normal structure. The reduction in χ values from 473 (as-grown) to 0.12 (850 air annealed) further supports our argument.

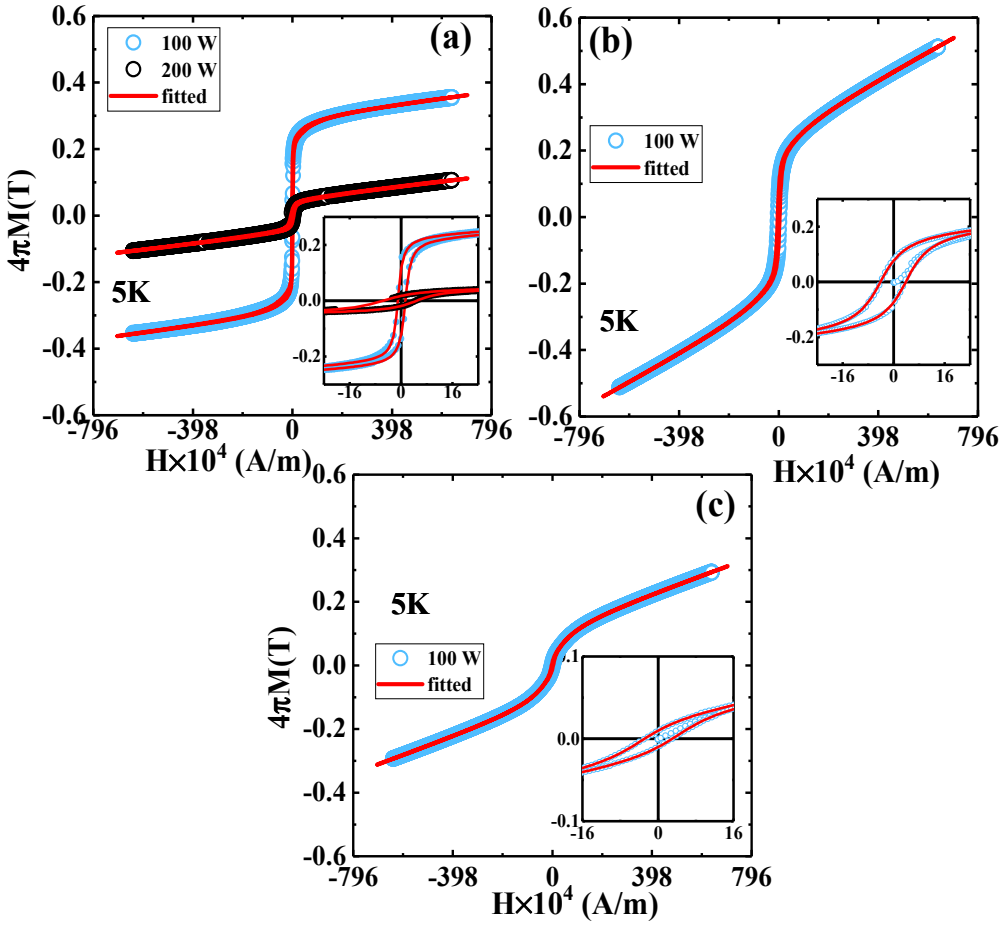

Figure 4. M−H loops (open symbols) for as-grown films (**a**) and films annealed at 500 °C (**b**) and 850 °C (**c**) along with fitted curves (solid lines). The insets show the low-field regions of M–H curves.

Table 2. Squareness ratio: $S = M_r/M_S$, saturation magnetization: M_S, magnetic susceptibility: χ, coercivity: H_C, and α^1 and α^2.

Sample	H_{C1} (kA/m)	H_{C2} (kA/m)	M_{Sf1} (T)	M_{Sf2} (T)	S_1	S_2	α^1	α^2	$1-\alpha^1-\alpha^2$	χ_f
as-grown 100 W	9.55	92.95	0.35	0.19	0.34	0.25	0.597	0.402	0.001	473
as-grown 200 W	45.67	446.111	0.048	0.02	0.20	0.13	0.984	0.001	0.016	0.47
100 W air annealed at 500 °C	38.28	42.73	0.39	0.21	0.31	0.17	0.251	0.636	0.112	0.32
100 W air annealed at 850 °C	14.40	36.37	0.16	0.13	0.06	0.03	0.105	0.722	0.173	0.13
100 W vacuum annealed at 500 °C	35.5	32.06	0.063	0.16	0.15	0.41	0.452	0.52	0.003	0.12

To shed light on the nonsaturation behavior in air-annealed samples, first, the high fields magnetization data were fitted to the Chikazumi law [24] of approach for saturation with expression $M(H) \propto (1 - a/H^n)$. The experimental data do not fit well with it, ruling out the possibility that factors such as defects and atomic anisotropy fluctuation can be the origin of this nonsaturation effect; alternatively, the PM contribution appears to be responsible for this high-field, nonsaturation behavior. We further notice that the FM contribution in as-grown films is composed of both soft (low H_C and high M_S) and hard part (high H_C and low M_S) ferrimagnetic phases. The soft part is attributed to the FM grain contribution, in which anisotropy gradually increases upon cooling in the inverted spinel while the hard part belongs to the SPM grain, in which larger changes in H_C and S can be observed below the blocking temperature due to increased effective anisotropy. With an increasing annealing temperature, the contribution of α^2 vs. α^1 increases because now the SPM grain grows to the FM, and the FM grain tends to the PM grain. Similar behavior

is also observed in 200 W films; it appears that both a high annealing temperature and high sputter power act as sources of thermal energy. Thus, air annealing is a good way to enhance the magnetic properties of sputtered films while retaining the stoichiometric Zn-ferrite phase. These results are different and stand out from reported spinel ferrite films where reasonably good magnetization can only be obtained at high-growth temperatures compared to our Zn-ferrite films grown at room temperature with post-thermal treatment.

In the second experiment, we analyzed the magnetic behavior of in situ vacuum-annealed (500 °C) Zn-ferrite films. Vacuum annealing is regarded to enhance ferrimagnetic properties, as suggested by many reports [7,31,32]. The FC magnetization behavior for in situ vacuum-annealed (500 °C) Zn-ferrite films is plotted in Figure 5a; it shows an anomaly below 130 K, which deviates from typical ferrimagnetic behavior as represented in the red dashed line (Bloch $T^{5/2}$ law [27]). We attribute the source of this anomaly to the presence of Fe^{+2} ions, which are believed to be produced during annealing in the reducing atmosphere (vacuum) because of the partial transformation of Fe^{+3} ions into Fe^{+2} ions at octahedral B sites of Zn-ferrite, such as $[(Zn^{2+})_{1-x-y}(Fe^{3+})_{x+y}]_A[(Zn^{2+})_x(Fe^{2+})_y(Fe^{3+})_{2-x-y}]_B(O^{2-})_{4-\delta}$. The M−H loops (see Figure 5b) of these films exhibit lower saturation magnetization M_S values (Table 2), which further indicates certain changes in the valance state of Fe. Particularly, the low M_S values can be linked to the presence of Fe^{+2} as Fe^{+2} has a lower spin magnetic moment of 4 μ_B compared to 5 μ_B of Fe^{+3}. It is worth noting that the lower lattice constant of 8.41 Å was observed for the vacuum-annealed sample, which further supports the argument about the presence of Fe^{+2} ions as it can induce structural shrinkage [31,32]. This cation inversion scheme is different not only from our ex situ air-annealed Zn-ferrite films $[Zn_{1-x}{}^{+2}Fe_x{}^{+3}]_A[Zn_x{}^{+2}Fe_{2-x}{}^{+3}]_BO_4$ of the same annealing temperatures (see Table 2) but also from $Zn_xFe_{3-x}O_4$:$[Zn_x{}^{+2}Fe_{1-x}{}^{+3}]_A[Fe_{1+x}{}^{+3}Fe_{1-x}{}^{+2}]_BO_4$ (see Figure 6), in which magnetization values normally increase if Zn contents decrease upon heat treatment, particularly in a reducing atmosphere [8,25,31,32]. The anisotropy constant of induced Fe^{+2} ions normally changes its sign ($K_1 > 0$) and also increases in value at the isotropic point ~130 K, which we suppose is responsible for the drop of magnetization values in the FC data. The change of sign in K_1 can occur at a particular temperature for the mixed-valence magnetite, $[Fe^{3+}]_A[Fe^{2+}Fe^{3+}]_BO^{2-}{}_4$ [33–37], with the maximum allowable concentration of Fe^{2+} ions, as reproduced in Figure 5a for reference. However, if the amount of Fe^{2+} concentration is decreased (by partial oxidation), this change in sign would occur at lower temperatures. At an isotropic point, the magneto-crystalline easy axis is reported to change from a <111> to <110> direction in the magnetite, but the crystal structure remains cubic [34–37].

To further verify the observed anomaly is related to the change in the valance state of Fe, that is, the presence of Fe^{+2} ions as a controlled experiment, we also sputtered magnetite films from the hematite (Fe_2O_3) target under similar growth and annealing conditions of Zn-ferrite films. Strikingly, we found an analogy of magnetization drop below 130 K in FC magnetization curves (see inset of Figure 5a) of magnetite films, albeit with higher net magnetization values in the entire temperature range. Thus, this study infers that the magnetic properties of nanocrystalline Zn-ferrite films are extremely sensitive not only to growth conditions but also postannealing treatments and their environment, leading to different types of grain sizes, Fe^{2+}/Fe^{3+} ratios, and magnetic interactions [32,38–40].

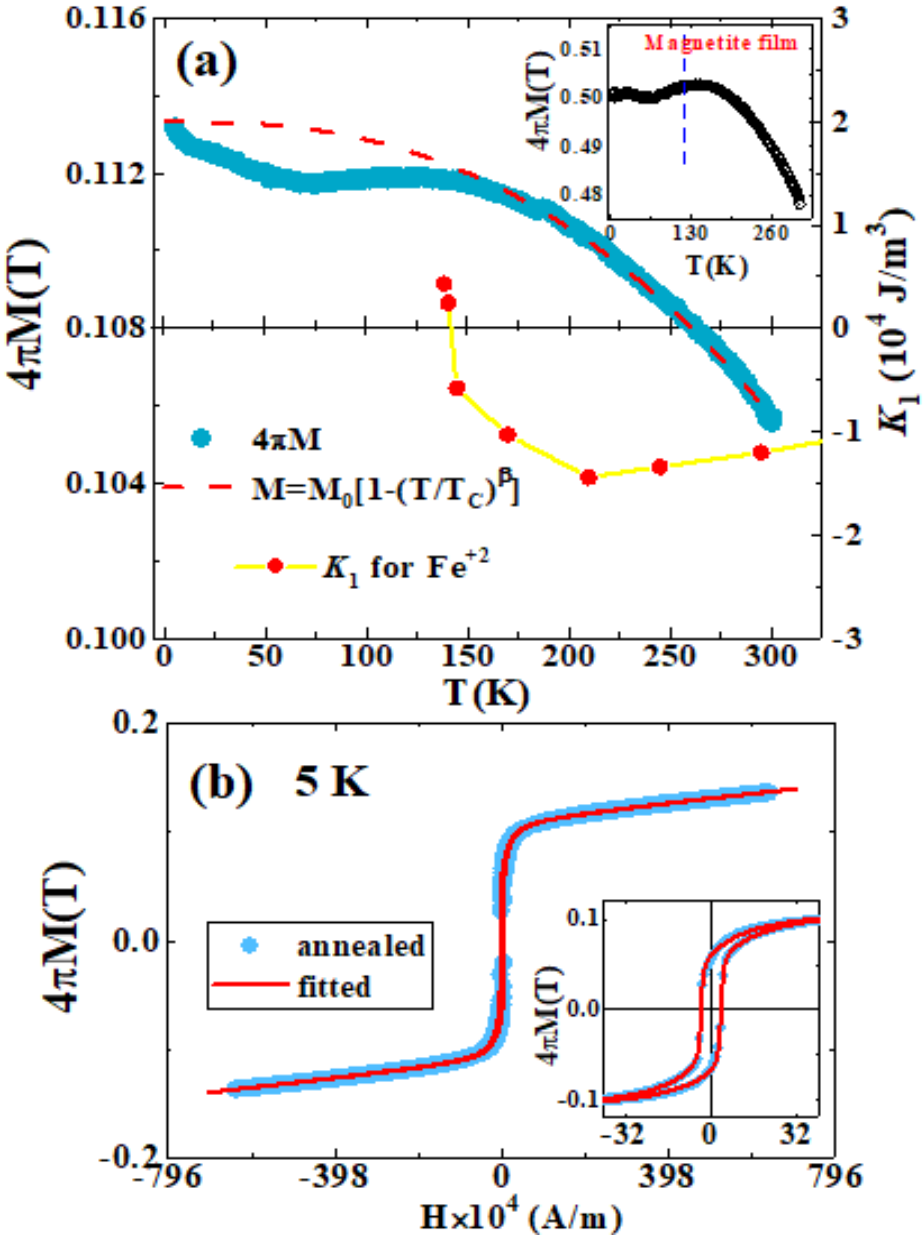

Figure 5. The M-T curve measured at 1.59 × 10^6 A/m for vacuum-annealed Zn-ferrite films (**a**). Red dashed lines indicate fitted data to the Bloch law. The red color closed symbol data for the K_1 anisotropy constant of magnetite was taken from reference [36]. The inset shows the M-T curve of magnetite thin films. The M−H loops of vacuum-annealed Zn-ferrite films were taken at 5 K (**b**).

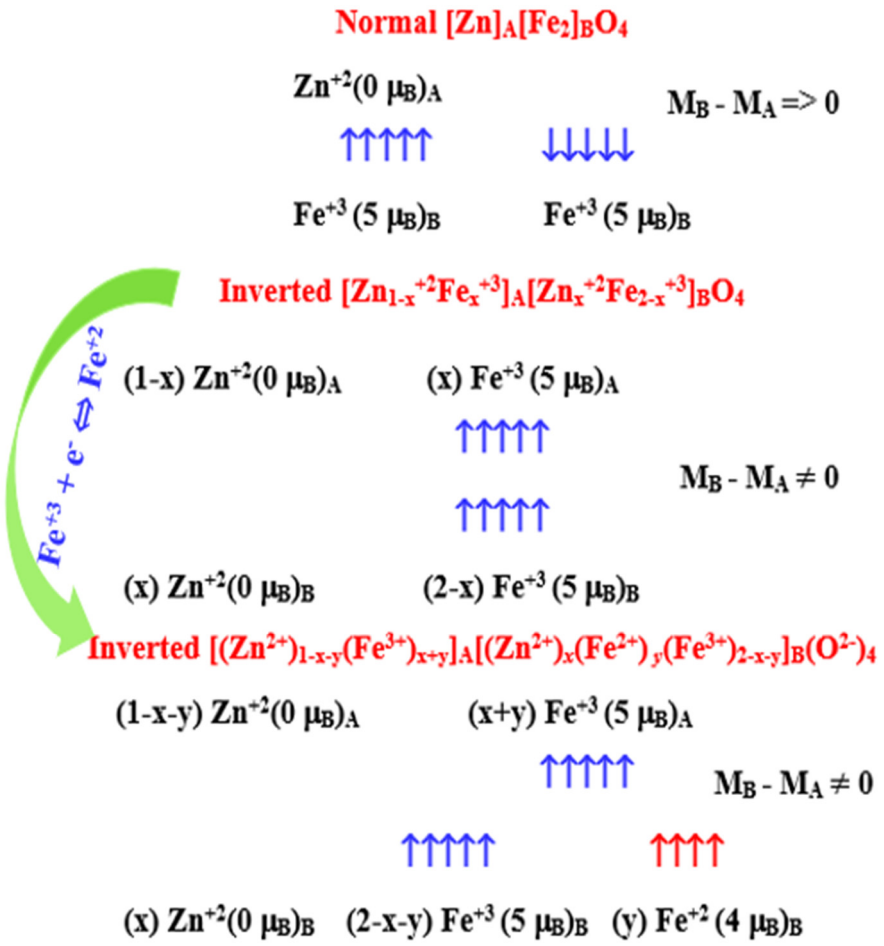

Figure 6. Various spin arrangement schemes in $ZnFe_2O_4$.

4. Conclusions

This research was aimed at interpreting the underlying magnetism of nanocrystalline Zn-ferrite thin films, which is commonly referred to as an antiferromagnet in its bulk form. Distinct forms of in situ and ex situ annealing procedures were used on these films, each of which caused cation inversion in the Zn-ferrite spinel structures in a different way. The following main conclusions can be drawn from the present study.

- By employing the component (SPM, FM, and PM) model, we successfully explained the temperature- and field-dependent magnetic properties of sputtered Zn-ferrite thin films, suggesting that the model may be the most appropriate for multicomponent magnetic systems.
- Ex situ air annealing changes the mixed dominance of the SPM and FM contributions to FM and, finally, bulk-type AFM state with increasing annealing temperature while preserving the single magnetic ion (Fe^{+3}) character.
- In situ vacuum annealing, on the other hand, results in a partial transformation of octahedral Fe^{+3} ions into Fe^{+2} ions, lowering the saturation magnetization value and causing an anomaly in low-temperature magnetization data around 130 K.
- Finally, because sputtered Zn-ferrite thin films have a low processing temperature and are easy to integrate with semiconductor technology, these tunable magnetic characteristics offer potential in spintronics and high-frequency devices.

Author Contributions: Conceptualization, M.B. methodology, B.S.; software, S.V.B. and N.S.; validation, M.B. and V.S.; formal analysis, M.B.; investigation, M.B.; resources, M.B.; data curation, M.B.; writing—original draft preparation, M.B.; writing—review and editing, A.A. and B.S.; visualization, M.B.; supervision, M.B.; project administration, M.B.; funding acquisition, M.B. All authors have read and agreed to the published version of the manuscript.

Funding: The authors acknowledge the International Bilateral Cooperation Division of DST, India for a grant under INT/BLG/P-14/2019 (India-Bulgaria Joint Research Projects scheme). The authors also acknowledge the Ministry of Science and Technology (MOST), Taiwan for financial support under Grants No. MOST-109-2112-M-110-012. We thank Shiva Prasad, Narayanan Venkataramani and Subasa Sahu from IIT-Bombay (India) for the use of few experimental facilities.

Institutional Review Board Statement: Not applicable.

Informed Consent Statement: Not applicable.

Data Availability Statement: Will be with author and can be provided upon request.

Conflicts of Interest: The authors declare no conflict of interest.

References

1. Bohra, M.; Alman, V.; Arras, R. Nanostructured $ZnFe_2O_4$: An Exotic Energy Material. *Nanomaterials* **2021**, *11*, 1286. [CrossRef] [PubMed]
2. Fritsch, D. Electronic and optical properties of spinel zinc ferrite: Ab initio hybrid functional calculations. *J. Phys. Condens. Matter* **2018**, *30*, 095502. [CrossRef] [PubMed]
3. Heda, N.L.; Panwar, K.; Kumar, K.; Ahuja, B.L. Performance of hybrid functional in linear combination of atomic orbitals scheme in predicting electronic response in spinel ferrites $ZnFe_2O_4$ and $CdFe_2O_4$. *J. Mater. Sci.* **2020**, *55*, 3912–3925. [CrossRef]
4. Ulpe, A.C.; Bauerfeind, K.C.; Bredow, T. Influence of spin state and cation distribution on stability and electronic properties of ternary transition-metal oxides. *ACS Omega* **2019**, *4*, 4138–4146. [CrossRef] [PubMed]
5. Kim, J.H.; Kim, H.E.; Kim, J.H.; Lee, J.S. Ferrites: Emerging light absorbers for solar water splitting. *J. Mater. Chem. A* **2020**, *8*, 9447–9482. [CrossRef]
6. Harris, V.G. Modern Microwave Ferrites. *IEEE Trans. Magn* **2012**, *48*, 1075–1104. [CrossRef]
7. Bohra, M.; Prasad, S.; Kumar, N.; Misra, D.S.; Sahoo, S.C.; Venkataramani, N. Large room temperature magnetization in nanocrystalline zinc ferrite thin films. *Appl. Phys. Lett.* **2006**, *88*, 262506. [CrossRef]
8. Zviagin, V.; Sturm, C.; Esquinazi, P.D.; Grundmann, M.; Schmidt-Grund, R. Control of magnetic properties in spinel $ZnFe_2O_4$ thin films through intrinsic defect manipulation. *J. Appl. Phys.* **2020**, *128*, 165702. [CrossRef]
9. Marcu, A.; Yanagida, T.; Nagashima, K.; Tanaka, H.; Kawai, T. Transport properties of $ZnFe_2O_{4-\delta}$ thin films. *J. Appl. Phys.* **2007**, *102*, 023713. [CrossRef]
10. Granone, L.I.; Ulpe, A.C.; Robben, L.; Klimke, S.; Jahns, M.; Renz, F.; Gesing, T.M.; Bredow, T.; Dillert, R.; Bahnemann, D.W. Effect of the degree of inversion on optical properties of spinel $ZnFe_2O_4$. *Phys. Chem. Chem. Phys.* **2018**, *20*, 28267–28278. [CrossRef]
11. Nakashima, S.; Fujita, K.; Tanaka, K.; Hirao, K. High magnetization and the high-temperature superparamagnetic transition with intercluster interaction in disordered zinc ferrite thin film. *J. Phys. Condens. Matter* **2005**, *17*, 137–149. [CrossRef]
12. Jedrecy, N.; Hebert, C.; Perriere, J.; Nistor, M.; Millon, E. Magnetic and magnetotransport properties of $Zn_xFe_{3-x}O_{4-y}$ thin films. *J. Appl. Phys.* **2014**, *116*, 213903. [CrossRef]
13. Rivero, M.; Campo, A.D.; Mayoral, Á.; Mazario, E.; Sánchez-Marcos, J.; Muñoz-Bonilla, A. Synthesis and structural characterization of $Zn_xFe_{3-x}O_4$ ferrite nanoparticles obtained by an electrochemical method. *RSC Adv.* **2016**, *6*, 40067–40076. [CrossRef]
14. Yu, G.; Peng, N.; Zhou, L.; Liang, Y.; Zhou, X.; Peng, B.; Chai, L.; Yang, Z. Selective reduction process of zinc ferrite and its application in treatment of zinc leaching residues. *Trans. Nonferrous Met. Soc. China* **2015**, *25*, 2744–2752. [CrossRef]
15. Cobos, M.A.; Presa, P.D.L.; Llorente, I.; Alonso, J.M.; García-Escorial, A.; Marína, P.; Hernando, A.; Jiménez, J.A. Magnetic phase diagram of nanostructured zinc ferrite as a function of inversion degree δ. *J. Phys. Chem. C* **2019**, *123*, 17472–17482. [CrossRef]
16. Singh, J.P.; Nandy, S.; Kim, S.H. Effect of thermal annealing on the film and substrate/film interface: The case of $ZnFe_2O_4$. *Appl Nanosci.* **2022**. [CrossRef]
17. Lin, W.J.; Chang, W.C.; Qi, X. Exchange bias and magneto-resistance in an all-oxide spin valve with multi-ferroic $BiFeO_3$ as the pinning layer. *Acta Mater.* **2013**, *61*, 7444–7453.
18. Sai, R.; Endo, Y.; Shimada, Y.; Yamaguchi, M.; Shivashankar, S.A. Oriented nanometric aggregates of partially inverted zinc ferrite: One-step processing and tunable high-frequency magnetic properties. *J. Appl. Phys.* **2015**, *117*, 17E511. [CrossRef]
19. Sai, R.; Shivashankar, S.A.; Yamaguchi, M.; Bhat, N. Magnetic nanoferrites for RF CMOS: Enabling 5G and beyond. *Electrochem. Soc. Interface* **2017**, *26*, 71–76. [CrossRef]
20. Bohra, M.; Prasad, S.; Venkataramani, N.; Kumar, N.; Sahoo, S.C.; Krishnan, R. Narrow ferromagnetic resonance line width polycrystalline Zn-ferrite thin films. *IEEE Trans. Magn.* **2011**, *47*, 345–348. [CrossRef]

21. Monsalve, J.G.; Ostos, C.; Ramos, E.; Ramírez, J.G.; Arnache, O. Insight into magnetic properties in zinc ferrite thin films by tuning oxygen content. *Curr. Appl. Phys.* **2021**, *22*, 77–83. [CrossRef]
22. Bohra, M.; Prasad, S.; Venkataramani, N.; Sahoo, S.C.; Kumar, N.; Krishnan, R. Low temperature magnetization studies of nanocrystalline Zn-ferrite thin films. *IEEE Trans. Magn.* **2013**, *49*, 4249–4252. [CrossRef]
23. Nakashima, S.; Fujita, K.; Tanaka, K.; Hirao, K.; Yamamoto, T.; Tanaka, I. Thermal annealing effect on magnetism and cation distribution in disordered $ZnFe_2O_4$ thin films deposited on glass substrates. *J. Magn. Magn. Mater.* **2007**, *310*, 2543–2545. [CrossRef]
24. Dash, J.; Prasad, S.; Venkataramani, N.; Krishnan, R.; Kishan, P.; Kumar, N.; Kulkarni, S.D.; Date, S.K. Study of magnetization and crystallization in sputter deposited LiZn ferrite thin films. *J. Appl. Phys.* **1999**, *86*, 3303–3311. [CrossRef]
25. Srivastava, C.M.; Shringi, S.N.; Srivastava, R.G.; Nanadikar, N.G. Magnetic ordering and domain-wall relaxation in zinc-ferrous ferrites. *Phys. Rev. B* **1976**, *14*, 2032–2040. [CrossRef]
26. Bohra, M.; Wu, C.P.; Yeh, H.J.; Cheng, Y.H.; Peng, C.C.; Chou, H. Role of Ru vacancies in the magnetism of strain relaxed $SrRuO_3$ films on $SrTiO_3$ substrates. *J. Appl. Phys.* **2011**, *109*, 07D728. [CrossRef]
27. Bohra, M.; Prasad, K.E.; Bollina, R.; Sahoo, S.C.; Kumar, N. Characterizing the phase purity of nanocrystalline Fe_3O_4 thin films using Verwey transition. *J. Magn. Magn. Mater.* **2016**, *418*, 137–142. [CrossRef]
28. Kamazawa, K.; Tsunoda, Y.; Kadowaki, H.; Kohn, K. Magnetic neutron scattering measurements on a single crystal of frustrated $ZnFe_2O_4$. *Phys. Rev. B* **2003**, *68*, 024412. [CrossRef]
29. Bohra, M.; Battula, S.V.; Alman, V.; Annadi, A.; Singh, V. Design of various Ni–Cr nanostructures and deducing their magnetic anisotropy. *Appl. Nanosci.* **2021**. [CrossRef]
30. Saha, R.; Srinivas, V.; Rao, T.C. Evolution of ferromagnetic like order in $Fe_2V_{1-x}Cr_xAl$ Heusler alloys. *Phys Rev B* **2009**, *79*, 174423. [CrossRef]
31. Philip, J.; Gnanaprakash, G.; Panneerselvam, G.; Antony, M.P.; Jayakumar, T.; Raj, B. Effect of thermal annealing under vacuum on the crystal structure, size, and magnetic properties $ZnFe_2O_4$ nanoparticles. *J. Appl. Phys* **2007**, *102*, 054305. [CrossRef]
32. Bohra, M.; Arras, R.; Bobo, J.-F.; Singh, V.; Kumar, N.; Chou, H. Multiple spintronic functionalities into single zinc-ferrous ferrite thin films. *J. Alloys Compd.* **2022**, *895*, 162425. [CrossRef]
33. Bickford, L.R., Jr. The Low Temperature Transformation in Ferrites. *Rev. Mod. Phys.* **1953**, *25*, 75. [CrossRef]
34. Ozdemir, O.; Dunlop, D.J. Low-temperature properties of a single crystal of magnetite oriented along principal magnetic axes. *Earth Planet. Sci. Lett.* **1999**, *165*, 229–239. [CrossRef]
35. Ozdemir, O. Coercive force of single crystals of magnetite at low temperatures. *Geophys. J. Int.* **2000**, *141*, 351–356. [CrossRef]
36. Muxworthy, A.R.; McClelland, E. Review of the low-temperature magnetic properties of magnetite from a rock magnetic perspective. *Geophys. J. Int.* **2000**, *140*, 101–114. [CrossRef]
37. Bohra, M.; Agarwal, N.; Singh, V. A Short Review on Verwey Transition in Nanostructured Fe_3O_4 Materials. *J. Nanomater.* **2019**, 8457383. [CrossRef]
38. Zhang, H.; Wang, Y.; Wang, H.; Huo, D.; Tan, W. Room-temperature magnetoresistive and magnetocaloric effect in $La_{1-x}Ba_xMnO_3$ compounds: Role of Griffiths phase with ferromagnetic metal cluster above Curie temperature. *J. Appl. Phys.* **2022**, *131*, 043901. [CrossRef]
39. Wang, H.; Zhang, H.; Wang, Y.; Tan, W.; Huo, D. Spin glass feature and exchange bias effect in metallic Pt/antiferromagnetic $LaMnO_3$ heterostructure. *J. Phys. Condens. Matter* **2021**, *33*, 285802. [CrossRef]
40. Wang, H.; Zhang, J.; Jia, Q.; Xu, F.; Tan, W.; Huo, D.; Gao, J. Three-dimensional strain state and spacer thickness-dependent properties of epitaxial $Pr_{0.7}Sr_{0.3}MnO_3/La_{0.5}Ca_{0.5}MnO_3/Pr_{0.7}Sr_{0.3}MnO_3$ trilayer structure. *J. Appl. Phys.* **2014**, *115*, 233911. [CrossRef]